Microstructure modeling of the dynamic recrystallization kinetics during turbine disc forging of the nickel based superalloy Allvac 718Plus^{TM}

D. Huber[1], C. Stotter[1], C. Sommitsch[1,2], S. Mitsche[3], P. Poelt[3], B. Buchmayr[2], M. Stockinger[4]

[1]Christian Doppler Laboratory of Materials Modelling and Simulation, Franz-Josef-Str. 18, A-8700 Leoben, Austria
[2] Chair of Metal Forming, University of Leoben, Franz-Josef-Str. 18, A-8700 Leoben, Austria
[3] Institute for Electron Microscopy, Graz University of Technology, Steyrerg. 17, A-8010 Graz, Austria
[4] Boehler Schmiedetechnik GmbH & Co KG, Mariazeller Str. 25, A-8605 Kapfenberg, Austria

Keywords: Allvac 718Plus^{TM}, Simulation, Microstructure, Dynamic Recrystallization

Abstract

The outstanding mechanical properties of the nickel based superalloy Allvac 718Plus^{TM} are sensitive to the microstructure, in particular to the grain size, which depends on the processing history. The grain structure is mainly controlled by thermo-mechanical processes like recrystallization and grain growth. This paper deals with the simulation of the evolution of the grain structure in alloy Allvac 718Plus^{TM} during disc forging using the Finite Element (FE) code Deform 2D^{TM}. Additionally the material flow, pressing forces and temperatures are of interest. The hot deformation behaviour of Allvac 718Plus^{TM} has been characterized in a temperature range of 900–1050 °C and at strain rates of 0.1–10 s^{-1} by use of cylindrical compression tests. Particular emphasis is put on the identification of the parameters of a semi-empirical model for dynamic recrystallization. Furthermore the simulated results are compared with an industrial trial-forging. The results of the simulations shall be the basis for the development of an optimized forging process with respect to cost effectiveness, product quality and low energy consumption.

Introduction

Aerospace gas turbine disks operate in an environment of relatively high stresses caused by centrifugal forces and elevated temperatures. These severe conditions necessitate the need for materials with high temperature strength and good low cycle fatigue resistance. One class of alloys used for this task are the nickel based superalloys, out of which, Alloy 718 is the most widely used in the aerospace industry. A new grade Allvac 718Plus^{TM} shall further enhance the high temperature properties [1]. Its properties are attributed to the combined effects of the chemistry,

heat treatment as well as the microstructure. The ability to precisely control the microstructure development during forging needs sound process models, which provide reliable process conditions where no damage or flow instabilities occur. The objective of this work is the prediction of both the microstructure due to dynamic recrystallization and the process control parameters, i.e. temperature and strain rate, during hot closed die forging with the FE code Deform 2D^{TM}.

Experimental

Triple melt (VIM + ESR + VAR) nickel based superalloy Allvac 718Plus^{TM} with a billet size of 8" (203.3 mm) and an initial mean grain size of 20 μm was investigated in this study. The chemical composition in wt.% is shown in Table 1. Cylindrical compression samples with Rastegaev

Table 1: Chemical composition of Alloy 718Plus^{TM} in wt.%

C	Cr	Mo	W	Co	Fe
0.02	18.00	2.70	1.00	9.00	10.00

Nb	Ti	Al	P	S	Ni
5.50	0.75	1.45	0.006	0.006	Bal.

geometry and 16 mm diameter d_0 as well as 24.6 mm length, as shown in Fig. 1, were used. In order to reduce contact friction and to get homogeneous deformation a special glass powder was filled in the pockets of the samples. The recrystallization kinetics was studied by using compression tests under isothermal conditions at constant true strain rates at a Servotest thermo-mechanical treatment simulator (TMTS). The specimens were de-
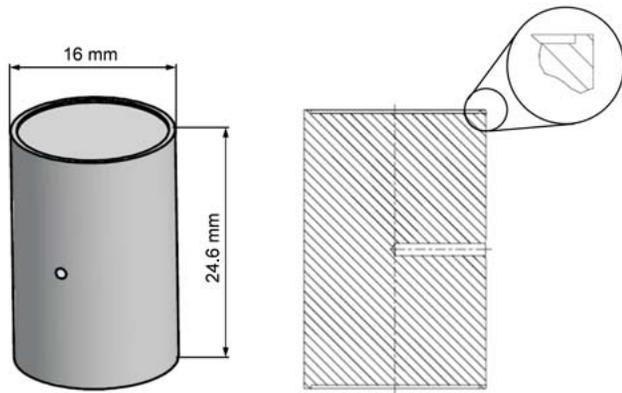
Figure 1: Dimensional sketch of the Rastegaev sample.

formed in a temperature range of 900–1050 °C at constant strain rates of 0.1–10 s^{-1} to different true strains of 0.2, 0.4, 0.6, 0.9 and 1.6. Water quenching after compression retained the dynamically recrystallized microstructure. Fig. 2 shows the heating cycle for the compression tests. First the samples were heated in the fast thermo
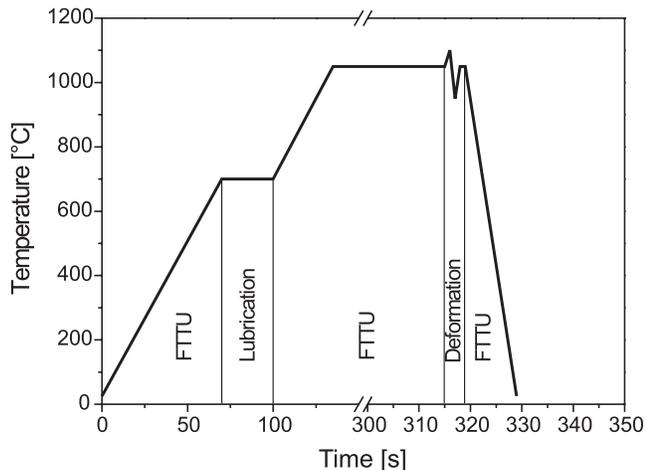
Figure 2: Heating cycle for the compression tests.

treatment unit (FTTU) inductively from room temperature to 650 °C at a heating rate of 10 °C/s^{-1}. Then the glass powder was attached to the Rastegaev samples' contact surfaces to reduce friction. After that samples were heated to forging temperature, e.g. 1000 °C, and held for 180 s at constant temperature. All tests were carried out in standard atmosphere. The transfer time of the sample from the FTTU to the press was 0.5 s. For mi-

crostructure investigations, the compressed samples were cut longitudinally (specimen center) and transversally (at a quarter of the specimen height). Finite element calculations of compression testing indicated that in this section from the centre to half of the radius, the local and the global strain rate correspond (see Fig. 3). It is neces-
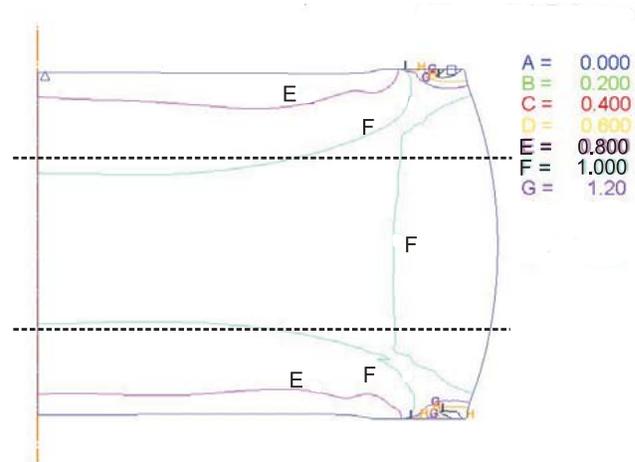
Figure 3: FE simulation for uniaxial compression (half-symmetrical longitudinal section); global strain rate = 1 s^{-1}, global strain = 0.9; corresponding global and local true strain at $\frac{1}{4}$ and $\frac{3}{4}$ specimen height (dashed line).

sary to prepare the samples metallographically and etch electrolytically. The recrystallized fraction and the final grain size were analyzed by using optical microscopy and verified by electron back scatter diffraction (EBSD) measurements.

EBSD measurements

The EBSD measurements and analyses were performed using an EDAX-TSL system (CCD-Digiview-camera, OIMTM 5.2 software) attached to a Zeiss Ultra FESEM (primary electron energy: 20 keV; probe current: 5.4 nA). In order to minimize the strain caused by the grinding and polishing processes the specimens were finally polished with an alkaline colloidal silica solution (OP-U suspension from Struers, 0.04 μm granularity) for 60 minutes. An area of 250 μm x 250 μm was scanned with a step size of 0.5 μm (hexagonal pixels). Grain boundaries were characterized by a misorientation larger than 5° between neighboring measurement points. To reduce the influence of noise in the results, a grain must comprise at least six pixels resulting in a minimum grain diameter of around

856

1.4 μm. The discrimination between the still deformed and the recrystallized grains were carried out with the grain orientation spread, because of the approved accuracy of this method [2].

Results

Isothermal flow curves

Data received from the TMTS were force versus stroke including both the elastic and the plastic region [3]. In a first step the elastic region was corrected. Finally flow stress σ and true strain ε were calculated by

$$\sigma = \frac{4Fh_i}{\pi h_0 d_0^2} \tag{1}$$

and

$$\varepsilon = \ln\left(\frac{h_0}{h_i}\right), \tag{2}$$

where h_0 is the initial height, h_i is the current height, d_0 is the initial sample diameter and F stands for the applied force.

The measured curves were adiabatic due to deformation heat (Fig. 4). To receive isothermal flow curves it is
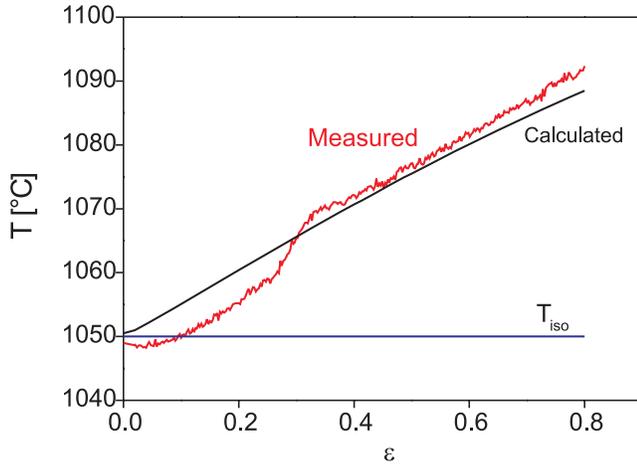
Figure 4: Measured temperature evolution in the specimen center compared to calculated values according to Eq.(3). The horizontal line represents the isothermal testing temperature T_{iso} (1050 °C in this case).

important to calculate the thermal influence on the flow stress. The increase in temperature depends on the mean flow stress $\bar{\sigma}$ in a deformation interval $\Delta\varepsilon$ and on the

thermo-physical properties of the material according to

$$\Delta T_d = k_T \frac{\bar{\sigma}}{\rho\, c_p}\, \Delta\varepsilon. \tag{3}$$

ΔT_d is the change in temperature during deformation (see Fig. 4), k_T is the fraction of deformation energy that dissipates in heat (≈ 0.9 for nickel-based alloys), ρ is the density and c_p is the specific heat capacity at constant pressure.

According to [4] the change in flow stress ($\Delta\sigma$ in Fig. 5) can be calculated by

$$\Delta\sigma = \left[\frac{\partial\sigma}{\partial(1/T)}\right]_{\Delta\varepsilon,\dot{\varepsilon}} \left[\frac{1}{T_{iso}+\Delta T_d} - \frac{1}{T_{iso}}\right]. \tag{4}$$

The term $\left[\frac{\partial\sigma}{\partial(1/T)}\right]_{\Delta\varepsilon,\dot{\varepsilon}}$ is the change of the flow stress with changing temperature at constant strain and constant strain rate. It was calculated by spline interpolation. Fig. 5 shows the comparison between an adiabatic and an isothermal flow curve.
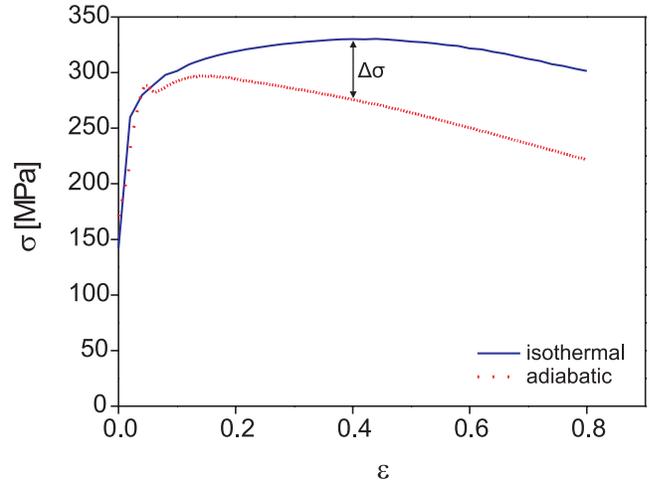
Figure 5: Strong decrease of flow stress due to temperature rise and material softening (adiabatic curve); compensated curve for isothermal conditions (isothermal curve) at $T = 1050$ °C and $\dot{\varepsilon} = 1$ s^{-1}.

Flow curve modeling

In metals with low stacking fault energy such as nickel-base alloys, recrystallization is the dominant softening mechanism during hot deformation. Reaching sufficiently

857

high local strains and temperatures leads to the nucleation and growth of new grains. The concurrent deformation stimulates an ongoing nucleation if a critical strain is reached. Thus the microstructure contains grains having different sizes and strains [5]. If the hardening rate equals the recrystallization rate, a stationary flow stress is reached. The maximum stress σ_p for a given temperature T and strain rate $\dot{\varepsilon}$ can be described by

$$\sinh(\alpha\sigma_p) = AZ^m, \tag{5}$$

where Z denotes the Zener-Hollomon parameter

$$Z = \dot{\varepsilon}\exp\left(\frac{Q}{RT}\right). \tag{6}$$

α, A and m are material constants, R is the molar gas constant. Hence follows for the determination of the activation energy Q (430.0 kJmol^{-1})

$$\ln[\sinh(\alpha\sigma_p)] = \frac{mQ}{RT} + Const. \tag{7}$$

From Fig. 6 it is obvious that at low temperatures
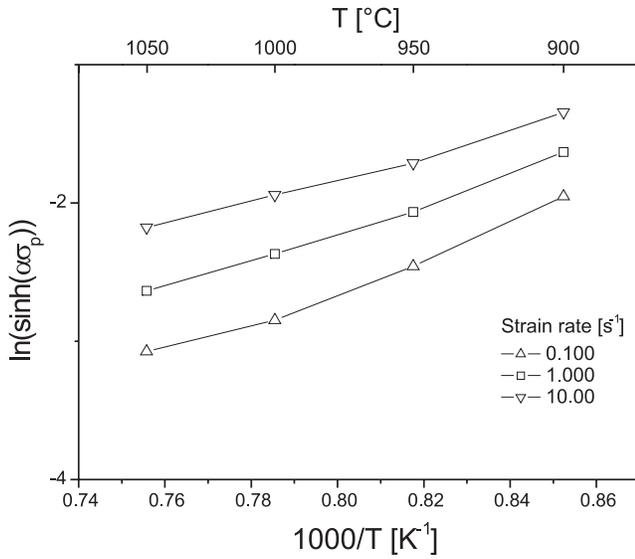
Figure 6: Arrhenius plot to calculate the activation energy Q for hot deformation according to Eq.(7).

(T<950 °C), the activation energy for hot deformation increases due to precipitation processes [6]. The values for α, A and m were determined with $2.26\cdot10^{-4}$, $2.55\cdot10^{11}$, 6.53, respectively.

The peak strain ε_p at σ_p depends on the initial grain size D_0 and Z [7]

$$\varepsilon_p = k_p D_0^{m_3} Z^{m_4}, \tag{8}$$

where k_p, m_3 and m_4 are material constants (Table 3). The influence of $\ln(Z)$ on $\ln(\varepsilon_p)$ is depicted in Fig. 7 for Allvac 718Plus^{TM}. Obviously, the different $\ln(\varepsilon_p)$–$\ln(Z)$ slopes for temperatures below and above the solvus temperature of the δ-phase ($T_\delta\approx$990 °C) in Allvac 718Plus^{TM} recommend the determination of two different parameter sets for both the flow stress and the DRX model.
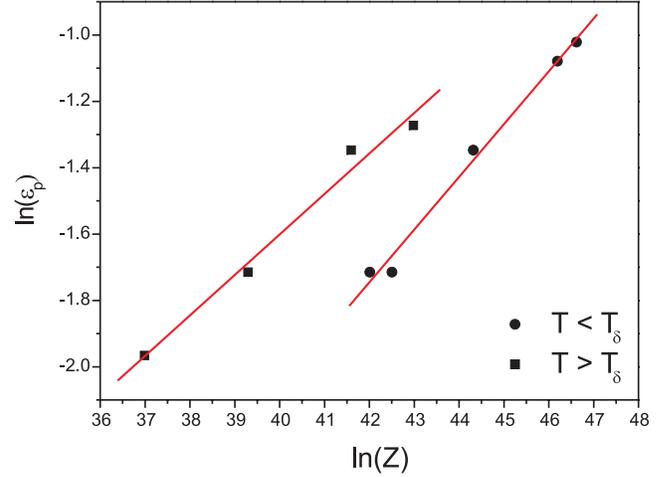
Figure 7: Variation of the slope $\ln(\varepsilon_p)$–$\ln(Z)$ above and below the solvus temperature T_δ of the δ-phase.

According to Karhausen [8], the $\sigma - \varepsilon$ relation in the hardening region of the flow curve can be described by

$$\frac{\sigma}{\sigma_p} = \frac{\varepsilon}{\varepsilon_p}\left[\exp\left(1 - \frac{\varepsilon}{\varepsilon_p}\right)\right]^C, \tag{9}$$

where the "work-hardening exponent" C can be described by

$$C = A_C\left[1 - \exp\left(-B_C \cdot \ln(Z)^{C_C}\right)\right], \tag{10}$$

$A_C(0.46)$, $B_C(3.97\cdot10^{-33})$ and $C_C(20.07)$ are constants.

Microstructure analysis

The evolution of the recrystallized fraction was measured by optical microscopy and EBSD analysis and showed good correlation for both methods. In the following the development of DRX exemplarily is shown for $T = 1000$ °C and $\dot{\varepsilon} = 1\ s^{-1}$. Fig. 8 depicts the increasing dynamic recrystallized fraction with increasing strain. Nucleation starts mainly at the grain boundary and leads to a typical necklace structure. A comparison of both DRX fraction measured by optical microscopy and EBSD analysis is shown in Table 2.

858
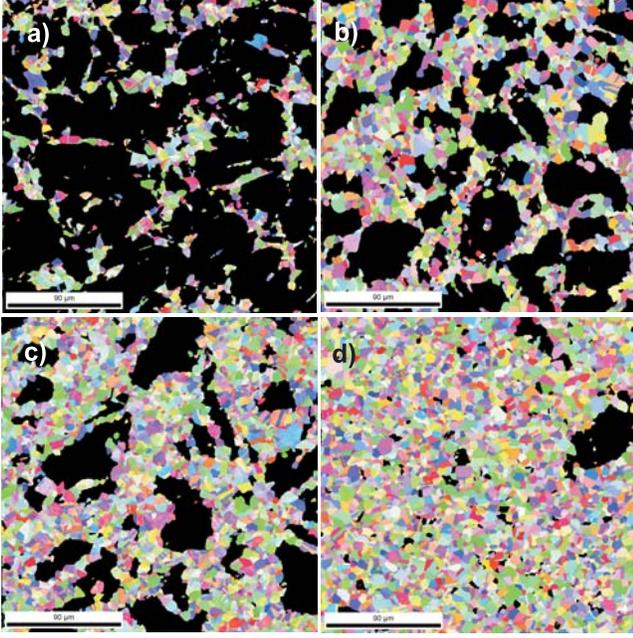
Figure 8: Progress of DRX at $T = 1000\,°C$ and $\dot{\varepsilon} = 1\ s^{-1}$ at strains of 0.4 (a), 0.6 (b), 0.9 (c) and 1.6 (d) based on EBSD analysis [2].

Table 2: Recrystallized fraction measured by optical microscopy (OM) and EBSD analysis at $T = 1000\,°C$ and $\dot{\varepsilon} = 1\ s^{-1}$ and different strains

ε	0.2	0.4	0.6	0.9	1.6
OM		0.32	0.50	0.68	0.98
EBSD	0.02	0.25	0.56	0.71	0.94

Dynamic recrystallization

Due to the high obtained strains during upsetting, the evolution of the microstructure between the start of recrystallization, close to the peak strain ε_p, and the steady state could be investigated. The dynamically recrystallized fraction X_{DRX} in general can be described using an Avrami type equation

$$X_{DRX} = 1 - \exp\left[\ln(0.5)\left(\frac{\varepsilon - \varepsilon_{cr}}{\varepsilon_{0.5} - \varepsilon_{cr}}\right)^{m_1}\right]. \quad (11)$$

Here the exponent m_1 is a constant, ε_{cr} and $\varepsilon_{0.5}$ denote the critical strain for the onset of DRX and the strain for 50% recrystallization, respectively:

$$\varepsilon_{cr} = k_{cr}\varepsilon_p, \quad (12)$$

where k_{cr} is 0.8 and

$$\varepsilon_{0.5} = k_1 Z^{m_2}. \quad (13)$$

Calculated and measured X_{DRX} showed a good correlation, which is demonstrated in Fig. 9. The dynamically
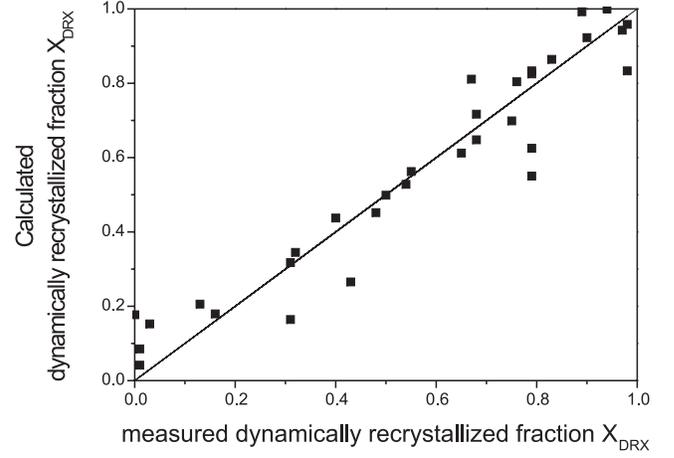
Figure 9: Calculated dynamic recrystallized fraction vs. measured dynamic recrystallized fraction. The 45° line represents full correlation.

recrystallized grain size D_{DRX} was found to follow the equation

$$D_{DRX} = k_2 \exp(Tk_3). \quad (14)$$

All parameters for the DRX model are given in Table 3.

Table 3: Model parameters for DRX kinetics. The influence of initial grain size was not considered, thus $m_3 = 0$

	k_p	k_1	k_2	k_3
$T < T_\delta$	$3.40 \cdot 10^{-3}$	$0.14 \cdot 10^3$	$0.4 \cdot 10^{-5}$	$1.10 \cdot 10^{-2}$
$T > T_\delta$	$3.40 \cdot 10^{-3}$	$3.45 \cdot 10^3$	$0.4 \cdot 10^{-5}$	$1.10 \cdot 10^{-2}$

	m_1	m_2	m_3	m_4
$T < T_\delta$	3.34	-0.11	0.00	0.10
$T > T_\delta$	0.88	-0.22	0.00	0.10

Industrial application

The described DRX model was implemented into FE code Deform 2D^{TM} using Fortran user routines. A four-step

859

disc forging was simulated to find optimal process conditions: Billet heating to forging temperature - two passes - reheating - two passes (Fig. 10). The heating tempera-
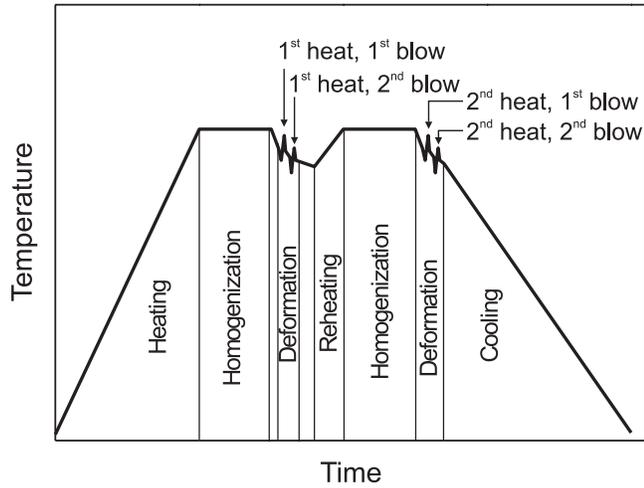
Figure 10: Schematic diagram of the four pass turbine disc forging process.

ture of the billet (203.2 mm diameter, 200 mm height) was $1000°$C and the initial mean grain size was assumed to be 20 μm. In Fig. 11 both the accumulated strain (Fig. 11a) and the DRX fraction distribution (Fig. 11b) after the fourth pass are shown. Finally FE simulations were compared with an industrial trial forging on a 31.5 Mt screw press. After the multi pass forging, an advanced dynamically recrystallized microstructure could be obtained both in the simulation and in the industrial process with a resulting grain size of 13 μm (ASTM 10) (see Fig. 11c). However, in the lower edge zone additional processes have a strong influence on the resulting grain structure, hence leading to differences between the measured and simulated grain size. The study thus stipulates further research according to static recrystallization during interpass.

Conclusion

The kinetics of dynamic recrystallization of the nickel based superalloy Allvac 718 Plus^{TM} was investigated in this work. Flow curves were measured in the process window of turbine disc closed die forging and were transformed to isothermal stress–strain plots. Out of those data, parameters for a mathematical flow curve description as well as an Avrami type dynamic recrystallization models were obtained by numerical regression.
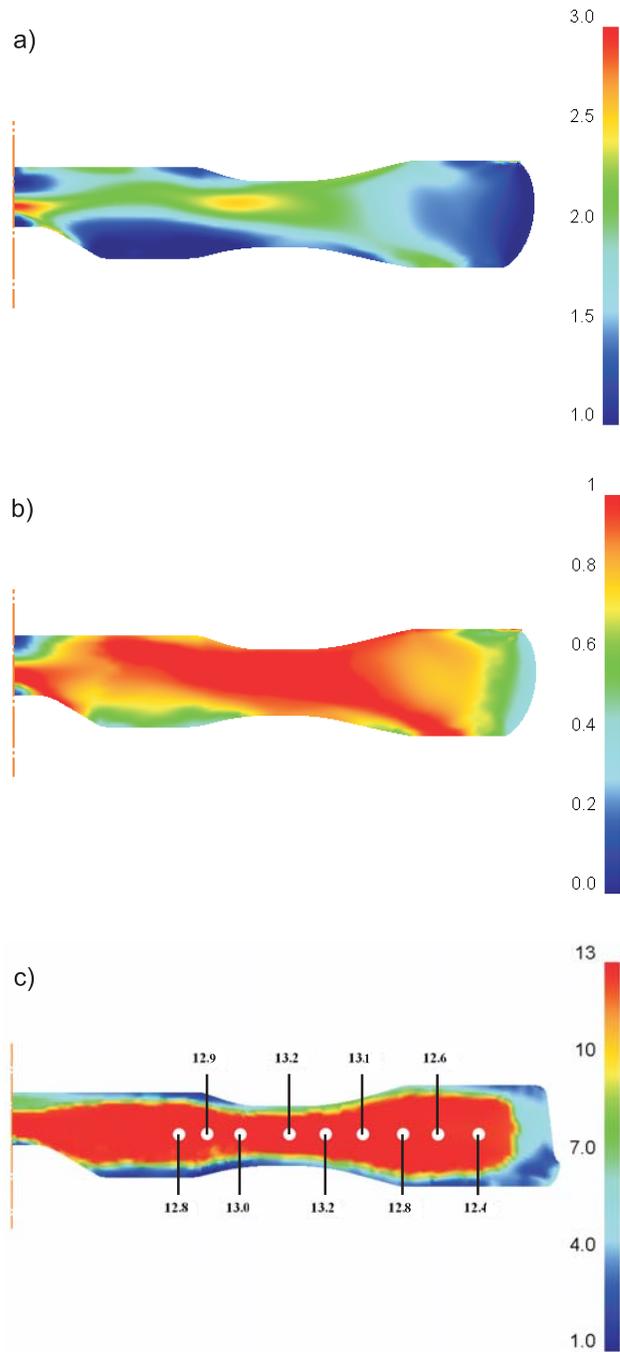
Figure 11: FE model (third pass) of a disc forging process. Accumulated true strain (a), the dynamically recrystallized fraction X_{DRX} (b) and the dynamically recrystallized mean grain size D_{DRX} [μm] (c) (after fourth pass) are shown.

The strong influence of the δ-phase Ni_3Nb on the softening behaviour of the material made it necessary to assign different parameter sets for both above and below the δ-solvus temperature. The metallographical investigations of the recrystallized fraction obtained by optical microscopy was validated by EBSD analyses, which showed a sound correlation. The semi-empirical model was implemented into FE code and was tested on a trial forging at industrial scale, which also showed good results. Further work will be done on static recrystallization that influences the grain size evolution of surface areas where small deformation occurred during the final pass.

References

[1] W.D. Cao, and R. Kennedy, "Role of chemistry in 718-type alloys – Allvac 718PLUS^{TM} alloy development", *Proc. Superalloys 2004*, ed. K.A. Green et al. (Warrendale, PA: The Minerals, Metals and Materials Society, 2004), 91.

[2] P. Poelt, C. Sommitsch, S. Mitsche, and M. Walter, "Dynamic recrystallization of Ni-base alloys - Experimental results and comparison with simulations", *Mat. Sc. Eng.*, A420 (2006), 306-314

[3] R. Kopp, R. Luce, B. Leisten, M. Wolske, M. Tschirnich, T. Rehrmann, and R.Volles, "Flow stress measuring by use of cylindrical compression test and special application to metal forming processes", *steel research*, 72 (2001), 394-401

[4] A. Laasraoui, and J.J. Jonas, "Prediction of steel flow stresses at high temperatures and strain rates", *Met. Trans.*, 22A (1991), 1545-1557.

[5] C. Sommitsch, and W. Mitter, "On modelling of dynamic recrystallisation of fcc materials with low stacking fault energy", *Acta Mater.*, 54 (2006), 357-375.

[6] C. Stotter, C. Sommitsch, J. Wagner, H. Leitner, I. Letofsky-Papst and M. Stockinger, "Characterisation of δ-phase in superalloy Allvac 718PLUS^{TM}", *Int. J. Mater. Res.* (2008), in press.

[7] C.M. Sellars, and J.A.Whiteman, "Recrystallization and grain growth in hot rolling", *Metal Sc.* 13 (1979), 187-194.

[8] J. Brand, K. Karhausen, and R. Kopp, "Microstrucural simulation of nickel base alloy Inconel 718 in production of turbine discs", *Mater. Sc. Techn.*, 12 (1996), 963-967